Selective Decoration of Metal Nanoparticles inside or outside of Organic Microstructures *via* Self-Assembly of Resorcinarene

Yan Sun, Yong Yao, Chao-Guo Yan,* Ying Han, and Ming Shen*

College of Chemistry & Chemical Engineering, Yangzhou University, Yangzhou 225002, China

ABSTRACT A facile template method was described for the decoration of organic microtubes with various nanoparticles (NPs), which was achieved in a straightforward "mix" process in the presence of templates and resorcinarene-functionalized nanoparticles (AuNPs, AgNPs, PtNPs, and PdNPs). A combination of UV—visible spectra and Fourier transform-infrared spectroscopy, transmission electron microscopy, field emission scanning electron microscopy, X-ray diffraction measurements, contact angle experiment, and energy dispersive X-ray spectroscopy was used for analysis. Interestingly, it was found that NPs could be encapsulated into the microtubes during the process of resorcinarene self-assembly. As a model system, AuNP-loaded microtubes were investigated and discussed, and loaded nanoparticles with a narrow size distribution were observed. Furthermore, AuNP-decorated microsheets could also be obtained by the assembly of resorcinarene with hydrazide groups. Remarkably, it was also observed that the incorporated NPs could be redispersed by treating the NP-loaded microtubes, which made it possible to realize the uptake and release of given nanoparticles. This procedure was scalable to diverse resorcinarene-based self-assemblies and applicable to various metal nanoparticles that decorate by resorcinarenes.

KEYWORDS: resorcinarene · nanoparticles · selective decoration · microtube · microsheet

Recently, the synthesis of noble metal nanoparticles have attracted increasing interest because of their unique properties and promising applications.[1−8] The synthetic technique for fabricating nanoparticles involved the reduction of metal salts in the presence of a protective agent, which prevents the nanoparticles from aggregation and allows isolation of the nanoparticles.[9,10] A number of stabilizers have been discussed that are suitable for the prepartion of nanoparticles.[11−14] Among them, calixarenes have receieved much attention because of their potential application in both protecting and functionalizing nanoparticles[15−21] through cooperative, multidentate interactions.[22] Wei made a comprehensive and systematic investigation[23] of resorcinarene-grafted nanoparticles. Up to now, calixarene-encapsulated nanoparticles have been successfully obtained[24−27] and achieved remarkable success in many fields.[28−35] However, most of them were prepared in organic solvents because of the poor solubility of calixarene in aqueous media. Thus, only a few reports have described the preparation of calixarene-capped nanoparticles in water,[36−38] which limits their potential application in the future.

Nowadays, the coupling of materials systems on different length scales enables new ways to take advantage of unique properties of nanoscale materials. Therefore, the ability to connect nanoparticles to the macroscopic world creates the promise of numerous applications and the generation of new technologies.[39] Organic—inorganic micro-nanohybrid materials exhibit synergy[40−44] among the properties of their components and have found promising applications in various fields. For example, Jang *et al*. found that PMMA nanofibers containing silver nanoparticles had antibacterial properties against both Gram-negative and Gram-positive bacteria.[45] Among various methods for preparing composites with different NPs, the template method has proven to be a powerful technique. Besides that, it was reported that NPs could be incorporated into materials *via* self-assembly. For instance, Forster[46] *et al*. described magnetic nanoparticles assembled into the bilayer membranes of block copolymer vesicles and demonstrated that the vesicles took up enough nanoparticles to become magnetophoretic in external magnetic fields.

Here, we used resorcinarenes as a ligand for the fabrication of water-soluble noble nanoparticles including AuNPs, AgNPs, PtNPs, and PdNPs. In this way, one could

*Address correspondence to cgyan@yzu.edu.cn, shenming@yzu.edu.cn.

Received for review October 14, 2009 and accepted March 08, 2010.

Published online March 17, 2010. 10.1021/nn901412n

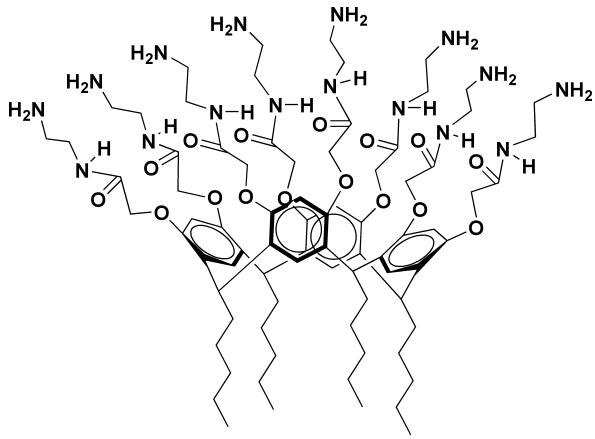

Scheme 1. Diagrammatic sketch of resorcinarene **C5−C2**.

decorate various resorcinarene-functionalized nanoparticles of the as-prepared microtubes. Remarkably, AuNPs could be encapsulated *via* the process of resorcinarene self-assembly, which resulted in the NPs locating on both the outside and inside of microtubes. Furthermore, by using resorcinarene hydrazide derivatives as the capping agent, AuNPs could be assembled into microsheets *via* the organization of their capping agents. It was also found that the obtained composites could be dispersed by sonication.

RESULTS AND DISCUSSION

Synthesis of Resorcinarene-Modified Metal Nanoparticles. The main goal of this work was the design and the synthesis of hierarchical micro-nanomaterials combining of metal nanoparticles and organic microtubes/microsheets. In our previous reports, we used amphiphilic polyamine resorcinarene **C11−C2**[47] with an eight-amino-head, a calixarence cavity, and four-undecyl-tail as ligand to prepare gold nanoparticles. Now, we developed a facile methodology for the aqueous synthesis of other noble metal nanoparticles by using resorcinarene **C5−C2**[47] as the protective agent. As shown in Scheme 1, **C5−C2** possesses similar structural features to **C11−C2**; the difference between **C11−C2** and **C5−C2** is the slight change in hydrophobic moieties. **C5−C2** possesses shorter alphatic chains than does **C11−C2** in the hydrophobic segment. However, it exhibits excellent properties in the encapsulation of nanoparticles as **C11−C2**.

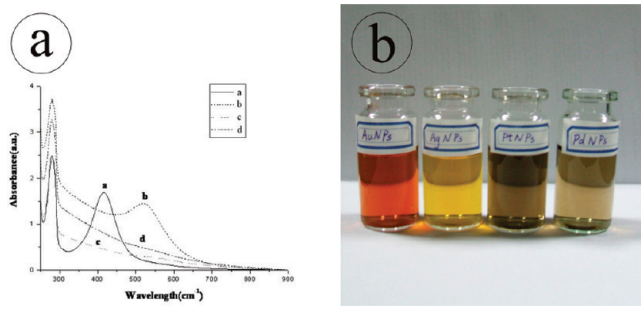

Figure 1. (a) UV−vis absorption spectra of Au, Ag, Pt, and Pd nanoparticles: (curve a) Ag, (curve b) Au, (curve c) Pt, (curve d) Pd nanoparticles. (b) Optical images of resorcinarene-functionalized metal nanoparticles.

AuNPs were prepared as follows: an aqueous solution of $HAuCl_4$ and **C5−C2** aqueous solution were mixed in a round flask. Then, sodium borohydride aqueous solution was injected into the above solution under vigorous stirring to give the resorcinarene-modified AuNPs. The formation of gold nanoparticles was verified by using a UV−vis spectrophotometer. Figure 1a (curve b) shows characteristic plasmon bands for the Au nanoparticles at 500−550 nm,[48] which confirm the existence of AuNPs. The reduction of silver ions in aqueous media yields AgNPs. Figure 1a (curve a) displays the corresponding UV−vis spectra of the as-obtained silver colloids, which exhibit characteristic plasmon bands for the Ag nanoparticles at 416 nm.[49] Furthermore, other noble metal nanoparticles used herein were prepared by reduction of the respective metal salts with sodium borohydride. The K_2PtCl_6 and **C5−C2** mixed solution was initially pale in yellow. After the addition of a reducing agent, the color of the solution changed to dark black, which was further monitored by UV−vis spectrophotometer. As shown in Figure 1a (curve c), the absorption band around 260−280 nm characteristic of the precursors was absent, suggesting that all $PtCl_6^{2-}$ ions were reduced by sodium borohydride, confirming the formation of a platium nanoparticle.[50] The disappearance of $PdCl_4^{2-}$ ions were observed by UV−vis spectra after the addition of the reducing agent, suggesting that the Pd nanoparticles formed.[51] And meantime, the solution exhibited a drastic color change from orange to dark brown accompanied with the change in observed spectra.

The optical images of as-prepared colloids match well with the UV−vis spectra. As shown in Figure 1b, the red and yellow color is attributed to the surface plasmon resonance of gold nanoparticles and silver nanoparticles. The obtained platinum and palladium nanoparticles show dark black and dark brown color, respectively. The colloidal dispersions of the resorcinarene-functionalized metal nanoparticles are stable for months at room temperature, indicating that resorcinarenes **C5−C2** are good stabilizing agents for Au, Ag, Pt, and Pd NPs.

Figure 2a shows an image of AuNPs observed by transmission electron microscopy (TEM), which reveals that the particles are spherical in shape, and each particle is well-separated. It could be seen that the nanoparticles with an average size of 5.9 nm are formed in the presence of **C5−C2**. The stable silver colloids protected by **C5−C2** are shown in Figure 2b. The average particle size of AgNPs is in the range 4.5−37.3 nm. Figure 2c shows a typical TEM image of PtNPs, which displays that the mean with standard deviation of the di-

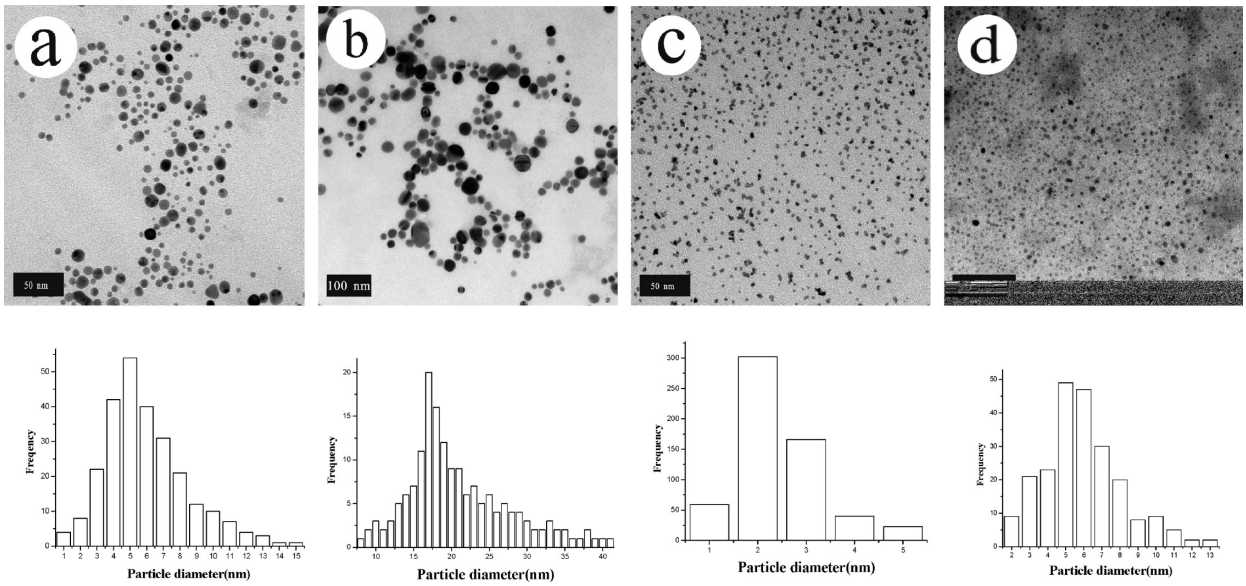

Figure 2. TEM images and size histograms (bottom) for the resorcinarene-stabilized metal nanoparticles: (a) gold nanoparticles, 5.9 ± 2.50 nm, (b) silver nanoparticles, 20.9 ± 16.4 nm, (c) platinum nanoparticles, 2.4 ± 0.9 nm, (d) palladium nanoparticles, 5.9 ± 2.2 nm.

ameter is about 2.4 ± 0.9 nm. However, the morphology of PtNPs synthesized is very different; most of them are well dispersed with a low degree of agglomeration. Figure 2d exhibits a typical TEM image and the corresponding size distribution of the PdNPs, which shows that resorcinarene-capped PdNPs had an average diameter of 5.9 nm with a standard deviation of 2.2 nm.

As shown in Figure 3a, FT-IR spectra of the **C5−C2**-capped metal nanoparticles support the presence of resorcinarene molecules on the metal nanoparticles in all of the studied cases. Powder X-ray diffraction (XRD) analysis was used to characterize the chemical composition. The pattern presented the AgNPs (Figure 3b) and exhibits diffraction peaks at $2\theta = 38.0°$, 44.2°, 64.3°, and 77.2° corresponding to the (111), (200), (220), and (311) crystal plane of Ag^0, respectively.[52] A typical XRD pattern of the Pt nanoparticles is shown in Figure 3c, which gives further support to the presence of Pt NPs. Four peaks at $2\theta = 39°$, 46°, 67°, 81° were found, which were assigned to the (111), (200), (220), and (311) reflections, respectively.[53] The formation of Pd NPs was also

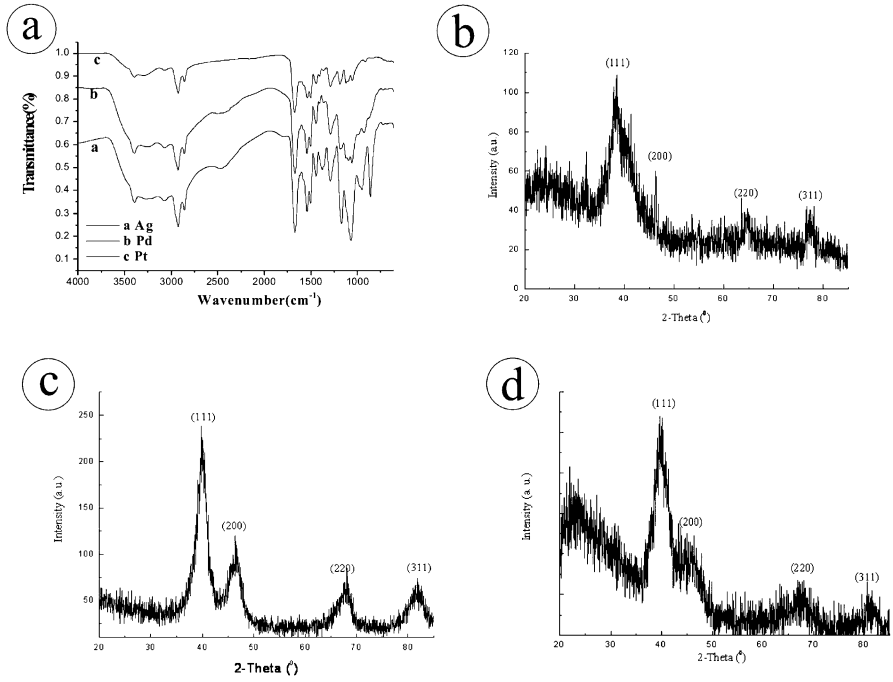

Figure 3. (a) FT-IR spectra of resorcinarene-functionalized metal nanoparticles; XRD of (b) silver nanoparticles, (c) platinum nanoparticles, (d) palladium nanoparticles coating the resorcinarene.

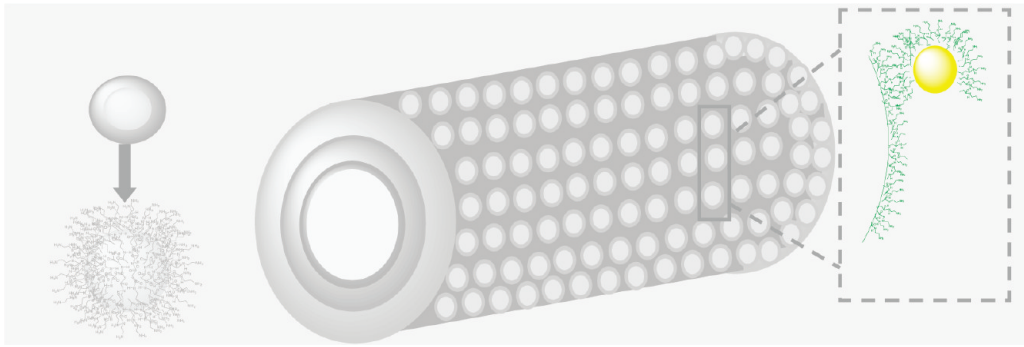

Scheme 2. Schematic illustrations of resorcinarene-capped NP-decorated microtube.

evidenced by XRD; four Pd diffraction peaks could be seen at around $2\theta = 40°$, 46°, 68°, and 81°, assigned to the (111), (200), (220), and (311) reflections of Pd, respectively (Figure 3d).[54]

It is essentially important to discuss the structure of aminoresorcinarene-modified NPs obtained. The aminoresorcinarene **C5−C2** was proven insoluble in common organic solvents, and the solubility in water was largely influenced by the protonation state of amino moieties. It is also worth mentioning that the uncharged species tend to form gel in water, whereas the fully protonated species with hydrochloric acid was soluble in water.[47] Partially protonated resorcinarenes are essential both as ligands for the nanoparticles and as building blocks for the microtubes preparation. In acidic water solutions, some of the amino groups of the resorcinarene were protonated. However, amido groups, which are usually not protonated, are important in the self-assembly process. In low pH cultures, amino groups of resorcinarene could easily integrate the H^+ to form the protonated amino-groups, which result in the electrostatic attraction forces between NH_3^+ of aminoresorcinarene and $AuCl_4^-$. Therefore, $AuCl_4^-$ ions added to the aqueous solution of resorcinarene would be coordinated onto the protonated amino-groups through coordination or electrostatic interactions to form the complex ion-pair $[-NH_3^+ - AuCl_4^-]$.[30,36,47] Accordingly, metal ions such as $PtCl_6^{2-}$ and $PdCl_4^{2-}$ are expected to bind preferentially to the surface amino groups, resulting in the formation of the resorcinarene−metal complex.[55] After the addition of sodium borohydride, resorcinarene−metal composites would be formed by adsorbing the resorcinarenes on the metal nanoparticles. Since the interactions between the metal particles and the functional groups of the aminoresorcinarenes are strong, such as gold/resorcinarenes with an amidoamine group, the obtained AuNPs have a small standard deviation and are well dispersed in the colloids. However, the particles show some aggregation behavior in the case of weak interaction between (PtNPs/PdNPs) and the functional groups, which supports the results of the previous literature reported by Kunio.[56] Although Ag^+ ions are not expected to interact strongly with the amino groups, amino-containing molecule−Ag^+ complexes that were also characterized by electron paramagnetic resonance analysis evidenced the strong complexion between amino groups and Ag^+ ions.[57] Thus, aminoresorcinarenes would cover the silver nanoparticles to stabilize the silver nanoparticles after the reduction. As a result, relatively large silver nanoparticles with a large standard deviation are only obtained. The average diameter with standard deviation determined from their histograms is 20.9 ± 16.4 nm, which is a result of a weak interaction of silver nanoparticles with the aminoresorcinarenes.

Fabrication of Hybrid Materials Composed of Metal NPs and Microtubes. ***Template Method.*** We have previously prepared AuNP/microtube hybrid materials by using microtubes as templates, which were obtained by the self-assembly of partially protonated aminoresorcinarenes (see Scheme 2).[47] Now we extend the method to the fabri-

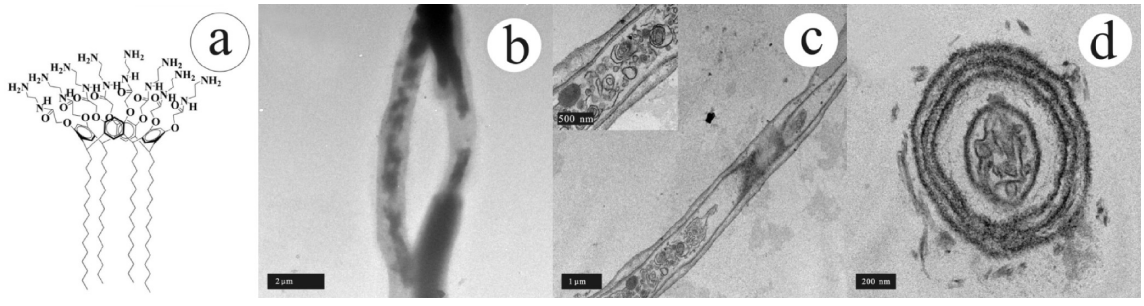

Figure 4. (a) The molecular structure of C15−C2. TEM images of (b) the C15−C2 microtube, (c) the profile section of the C15−C2 microtube with aggregates inside cylinder, inset image is the typical structure at greater magnification, and (d) the cross section of the C15−C2 microtube with vesicular aggregates encapsulated. The samples were prepared using the C15−C2 solution (150 μM) obtained after 1 month of incubation at room temperature.

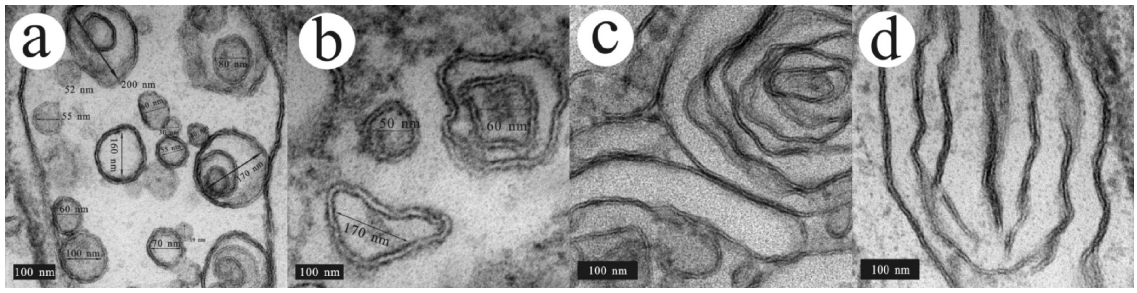

Figure 5. Cross section of (a) vesicles of varying size, (b) irregular vesicles, (c) disordered lamellar structure, (d) irregular lamellae.

cation of other noble metal hybrid materials by using the same microtubes as templates. Here we utilize the **C15−C2** (Figure 4a) with longer pentadecyl hydrophobic tails as a model molecule to fabricate templates. Figure 4b shows the observed tube with a diameter of 1.2 μm, which is in good agreement with the self-assembling behavior in our previous reports. Some small vesicular aggregates of varying size together with irregular bilayers inside the cylinder are also present (Figure 4c). The inset image represents higher magnification of the tube. The profile section of tube-wall in Figure 4d further confirms the previous observation. The images in Supporting Information, Figure S1 are in good aggrement with Figure 4. Approximately 500 microtubes are picked randomly from the TEM images to evaluate the distribution and average diameter of the tube. The size distribution of the tube is shown in Supporting Information, Figure S2, which reveals the assemblies with a mean diameter of 1.93 μm.

A wide range of nanoscale aggregates are often encountered in the system. Spherical vesicular structures of size varying from 19 to 200 nm are presented in Figure 5a. A small distorted vesicle within a larger one is shown in Figure 5b. The outer vesicle is 200 nm in diameter, and the inner one is 60 nm in diameter. Figure 5c exemplifies the disordered lamellar aggregates; Figure 5d displays the bilayers separated from each other. Compared to the nanostructure presented in previous reports,[47] our system now provides more complex and interesting structures (Supporting Information, Figure S3).

Further investigation may provide us with a deeper insight into the nature of the self-assembly. We detected some intermediates of the curly multilamellar structure gradually convert to a tube during the self-assembly, which suggests the possible mechanism of MT formation.[58−61] Figure 6a shows the cross section of a tube wall with 80 nm thickness. It is obvious that a multilamellar structure with 100 nm thickness is in the

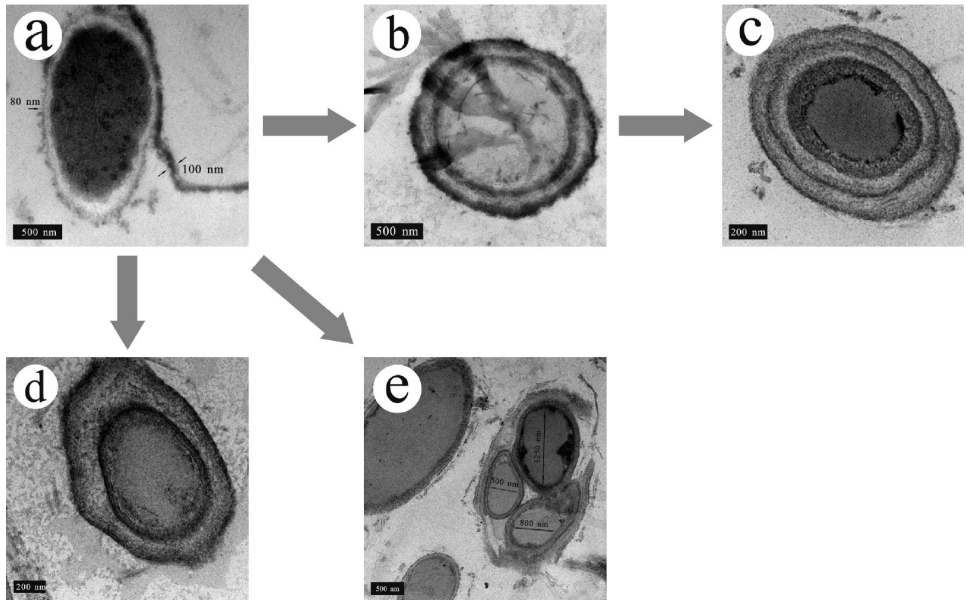

Figure 6. Possible intermediates of the curly multilamellar structure to multiwalled MT transition. Microtubule cross section with (a) curling multilamellar structure, (b) two continuous multilamellar structure, (c) three continuous multilamellar structure, (d) two multilamellar structure separated by water compartments, (b) MT containing three smaller tubes inside cylinder. The samples were prepared using the C15−C2 solution (150 μM) obtained after 1 month of incubation at room temperature.

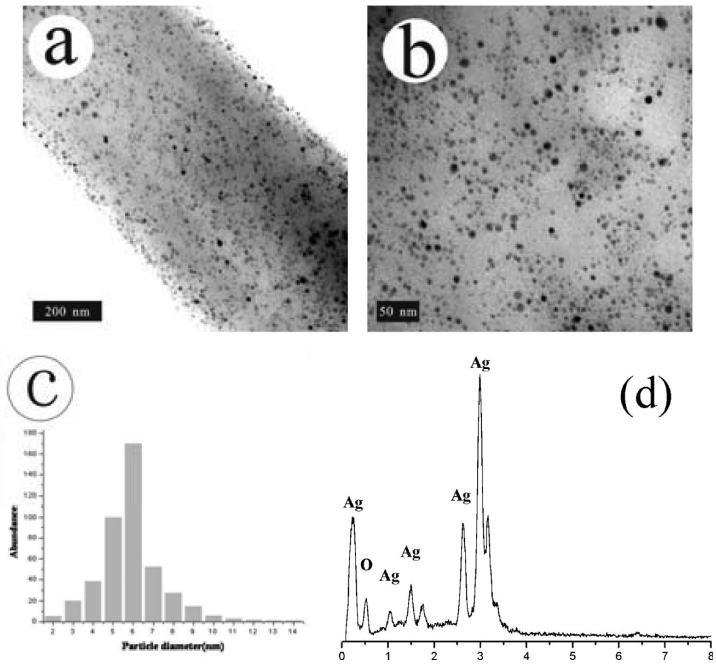

Figure 7. (a) TEM image of silver nanoparticles embedded on the surface of microtubes, (b) TEM image of these silver nanoparticles at higher magnification, (c) size distribution of AgNPs residing on the microtubes, (d) EDX profile of composites.

formation process. This observation is very important since it highlights the significance of a curled structure in the process of the MT's self-assembly. Figure 6b shows a MT with two multilamellar-walls. The further rolling-up of another multilamellar structure may result in the formation of the tube with three multilamellar-walls (Figure 6c). When a large amount of water is present, the MT walls consisting of two multilamellar structures separated by water compartments can be seen (Figure 6d). This structure might result from a following multilamellae curling outside the inner tube. Remarkably, MTs containing several smaller ones inside the cylinder are also observed (Figure 6e), which could result from the curling of a multilamellar structure around three smaller tubes. Different from the hollow tube displayed in Figure 6, when the vesicular structures or bilayer fragments are present during the curling process, nanoaggregate-containing multilamellar tube-walls could be observed (Supporting Information, Figure S4).

By comparing the spectra of the **C15−C2** powder sample with that of the microtube (Supporting Information, Figure S5), we observed the N−H stretching and carbonyl band of the powder at 3400 and 1674 cm^{-1} shift to 3304 and 1666 cm^{-1} in microtubes, respectively. The decrease of wavenumbers suggested the enhancement of the hydrogen-bonding in the microtubes. In addition, the antisymmetric and symmetric stretching vibrations of alkyl chains in the microtube were at 2923 and 2852 cm^{-1}, while the data of powder sample were at 2924 and 2853 cm^{-1}. Therefore, the interactions between alkyl chains of molecules also promoted the formation of the microtubes. The adsorption peaks of the amino and amido groups of **C15−C2** are affected by self-assembly, which indicates their participation in hydrogen bonding.[47] The mechanisms for the generation of MTs is suggested by molecular modeling of the MTs. It is proposed that two molecules initially undergo tail-to-tail packing to form a bilayer. Subsequently, the stacking of bilayers results in the formation of 2D sheets. Then, they grow into multilayers through continuous dynamic energy minimization. Finally, the flexible multilayers can subsequently roll-up *via* hydrogen bond leading to the generation of 1D MT.

We incubated a mixture of microtubes and Ag colloids. Within a few days, the suspension turned yellowish, which indicates the loading of silver nanoparticles.[62] Transmission electron microscopy was used to characterize the AgNPs attached to microtubes. Figure 7a clearly illustrates AgNPs with high loading density coating the microtubes. Images at higher magnification are presented in Figure 7b. Well-dispersed, spherical particles were anchored onto the surface of the microtube. It is should be noted that the diameter of these particles with narrow size distribution compared with freshly prepared. Their size distribution is shown in Figure 7c and indicates that the NPs with diameter of approximately 6 nm tend to be absorbed onto the surface. A characteristic energy-dispersive X-ray spectroscopy (EDX) profile for the composites is given in Figure 7d,

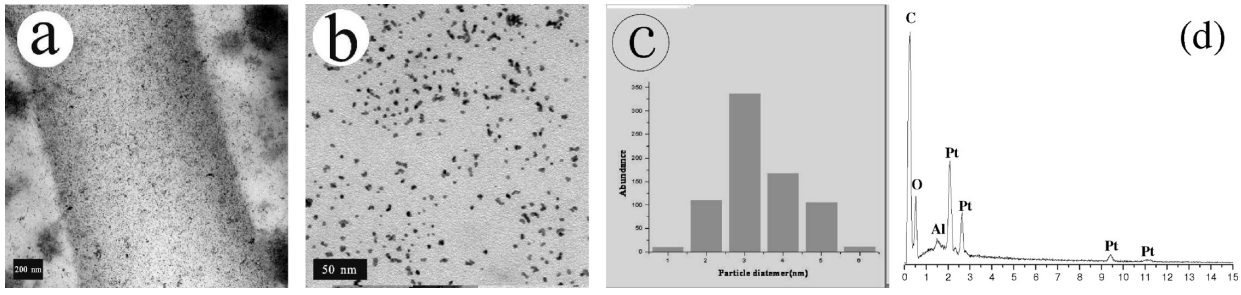

Figure 8. (a) TEM image of a self-assembled resorcinarene tube coated with Pt nanoparticles, (b) magnification of PtNPs on the composites, (c) size distribution of PtNPs residing on the microtubes, (d) EDX profile of composites.

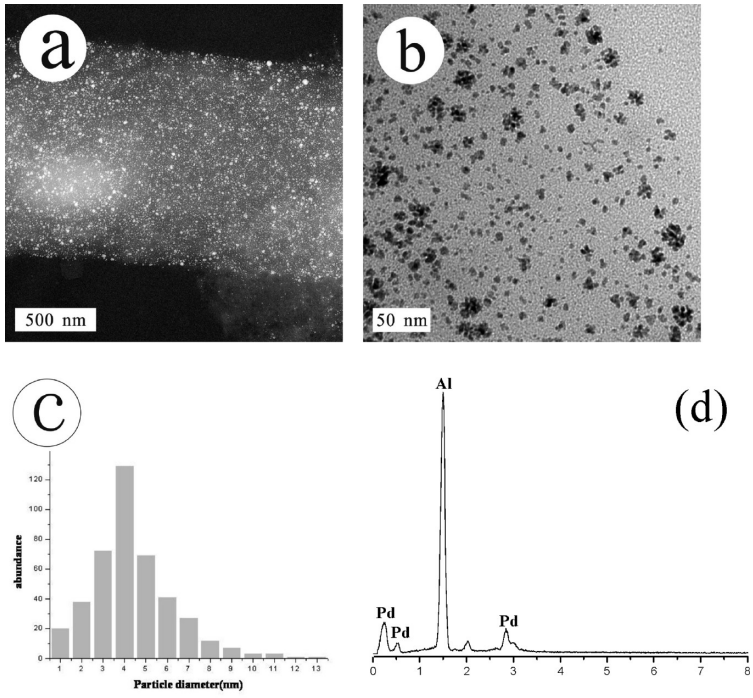

Figure 9. (a) TEM image of palladium nanoparticles embedded on the surface of microtubes, (b) TEM image of these palladium nanoparticles at higher magnification, (c) size distribution of PdNPs residing on microtubes, (d) EDX profile of composites.

which convincingly demonstrates the presence of AgNPs.[63]

A suspension of the microtubes is treated with platinum colloids and the loading was achieved after a few days. The initial white suspension turned black after PtNPs deposition with a mass uptake.[64] TEM image of the composites is shown in Figure 8a, which demonstrates that microtubes were densely covered by PtNPs. At high magnification (Figure 8b), the PtNPs can be visualized on the surface of tubes. Figure 8c shows the mean diameter with standard deviation of the Pt NPs was determined to be 3.4 ± 1.0 nm. An EDX spectrum of the composites confirmed the presence of Pt NPs.[65]

After the mixture of Pd colloids and microtubes aged at room temperature for several days, composites of PdNPs/microtubes were obtained. The color of the suspension was dark brown, which indicates the formation of hybrids. The TEM image in Figure 9a demonstrates the achievement of adsorption. Figure 9 panels b and c show a magnified image of PdNPs on a microtube and the corresponding histogram, which reveals that PdNPs have diameters of 4.3 ± 1.6 nm. An EDX profile (Figure 9d) further confirms the generation of Pd/microtube composites.[66]

According to the formation mechanism of microtubes previously reported,[47] the polar head groups displayed on the hydrophilic surface plays a special role for the immobilization of the NPs. From the above experiments, TEM provided clear information of how the NPs are capable of interacting with the microtube and then producing the coatings on the microtube. However, the close-ended microtubule prevents the resorcinarene-capped NPs from presenting on the interior surface of microtube. A schematic representation of the microtube is shown in Scheme 2. The resorcinarene-based microtube is covered with amidoamine groups outside and inside the surface. The microtube can adsorb the resorcinarene-modified NPs by the interaction between the amidoamine covered tubes and NPs, respectively.

The Shortcomings of the Template Method. The structure of composites under observation of FE-SEM (Figure 10, left) shows that the microtubes were coated with AuNPs. The composites obtained by template method (Figure 10, right) had diameters in the range of 250−700 nm. Importantly, NPs were only observed on

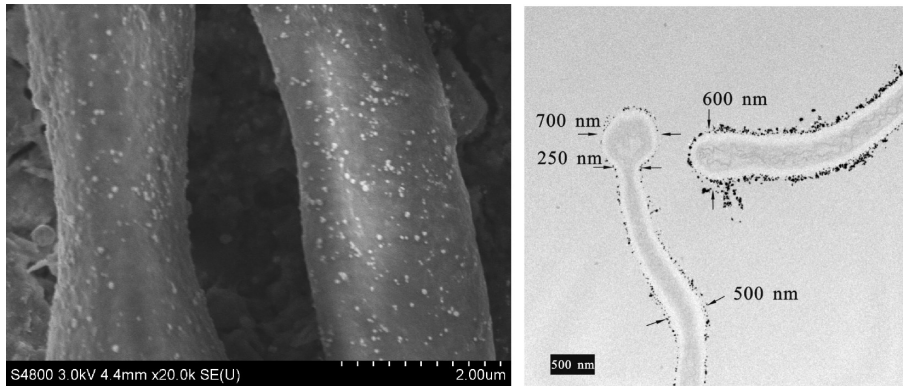

Figure 10. SEM image of AuNP-decorated microtube (left), the cross section of the AuNPs/microtube composites (right), which reveals the AuNPs only located on the exterior surface of microtubes.

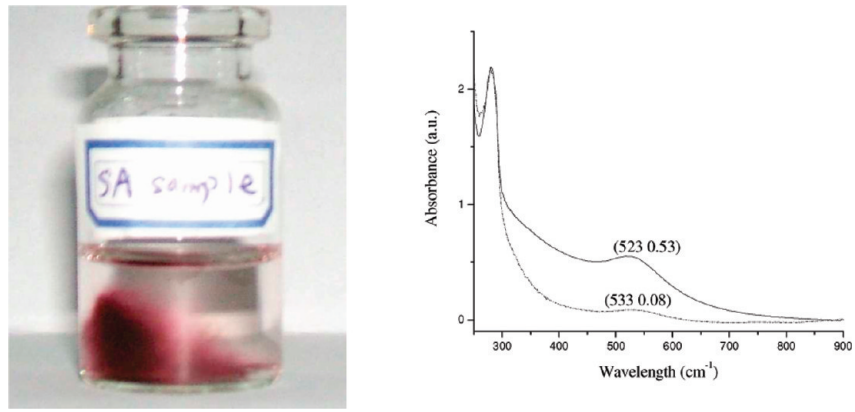

Figure 11. Digital image of the C15−C2 self-assemblies obtained in the presence of gold nanoparticles (left), UV−vis spectra of gold colloid before and after self-assembly (right).

the exterior surfaces of the tubes, which is in good agreement with our previous reports. The TEM image displays a cross section of an individual microtube (right). No AuNPs were found within the multilayer tube wall or inside the cylinders. A resorcinarene molecule has a mean size of approximately 3 nm, while the smallest AuNPs were larger than 5 nm, which prevented the AuNPs from diffusing into the microtube through the tube wall. Furthermore, it was clearly observed that the microtube ends are closed. Therefore, AuNPs could not enter the microtubes through the ends.

Co-assembly as Another Pathway for the Preparation of Hybrid Materials. ***Hybrid Tubular Micro-nanostructure.*** Because of this limit of the template method, the NPs were only located on the exterior surface. However, the inner surface and multilayer wall might also serve as sites for embedding NPs to form hybrid materials.

In this work, **C15−C2** was capable of self-assembling in colloids, which is similar to the self-assembly of pure resorcinarene; the major difference is the presence of NPs. To our surprise, AuNPs could be encapsulated in microtubes during the self-assembly process of resorcinarene. Figure 11 (left) shows a digital image of the **C15−C2** self-assembled in a gold colloid; soft, filamentous, wine-colored materials settled to the bottom of the bottle. The change in absorbance before (0.53) and after (0.08) self-assembly of **C15−C2** in the presence of AuNPs demonstrates that the characteristic optical signature typical of gold colloids was decreased with the process of assembly. As shown in Figure 11 (right), the plasmon resonance slightly shifts to lower energies as the AuNPs adsorb onto the microtubes. For this sample, the particles deposited on the tube are rather high, close to 85%. However, free NPs still exist in the solution.

Figure 12a shows a cross section of a typical AuNP-loaded microtube with an inner diameter of 800 nm and a wall thickness of 80 nm. Different from the hybrid materials obtained by the template method, the AuNPs bound not only on the surface but also in the sidewall. The micrograph also showed that the AuNPs remained isolated; they did not coalesce. Encapsulation might thus occur simultaneously at many sites in microtube walls, and many particles could locate within layers. AuNPs were incorporated into the wall through self-assembly of **C15−C2**, resulting in high nanoparticles density. Figure 12b shows an AuNP-loaded microtube with many vesicles inside the cylinder. It could be clearly observed that AuNPs were loading in the microtube-wall.

Notably, several bigger NPs were observed located at the exterior surface, which implies that only NPs with a certain size are prone to incorporation in the microtube by self-assembly. It should also be noted that not only did the AuNPs residing in the tube wall have a nar-

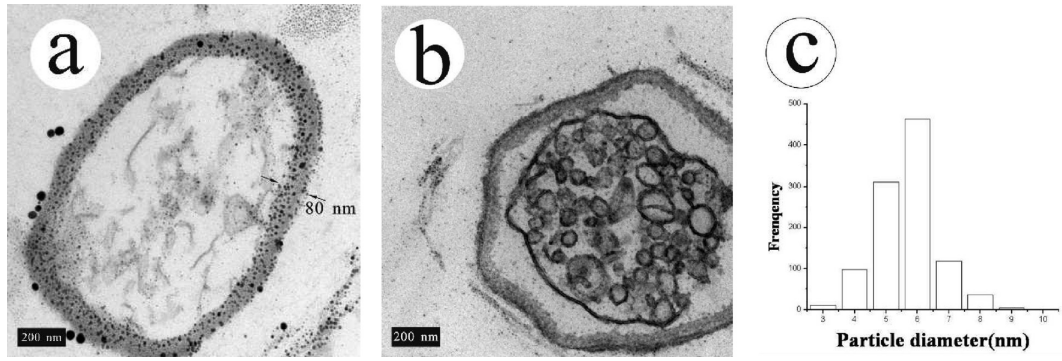

Figure 12. (a) Cross section of the AuNPs-loaded microtubes without aggregates inside the hollow cylinder; (b) cross section of AuNPs-loaded tube with many vesicles inside the cylinder; (c) size distribution of AuNPs.

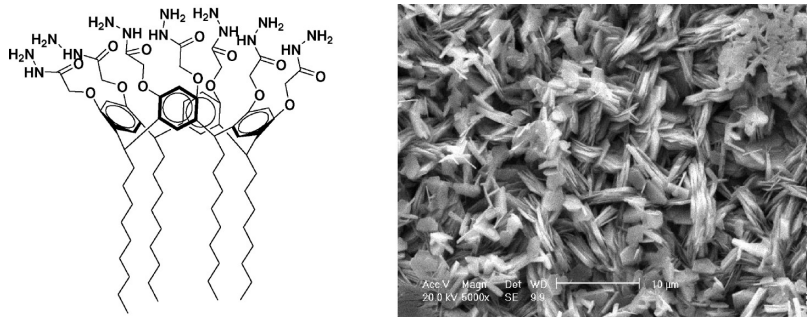

Figure 13. Diagrammatic sketch of resorcinarene C9−C0 (left), SEM image of microsheets assembled by C9−C0 (right).

row size distribution but also the AuNPs close to the hybrid materials had a uniform diameter of approximately 5 nm. The size distribution of the colloids, characterized by TEM, is illustrated in Figure 12c. The AuNPs had a mean diameter of 5 nm.

Besides AuNP-loaded microtubes, Ag, Pt, and PdNP-loaded microtubes can also be prepared by **C15−C2** self-assembly in the presence of AgNPs, PtNPs, and PdNPs, respectively. This will be reported in the near future. This method enables incorporation of various NPs into both the interior and exterior surface of microtubes.

Hybrid Sheet Micro-nanostructure. It was reported that microsheets could be obtained by the assembly of resorcinarene with hydrazide groups in hydrophilic moieties.[47] Now studies were conducted on other amphiphilic resorcinarene octahydrazide derivatives **C9−C0** (Figure 13), which have nonyl groups in the hydrophobic segment (left). Similar to our previous reports,[47] microsheets could be obtained by its assembly. By comparing the spectra of the **C9−C0** powder sample with that of the microsheet (Supporting Information, Figure S6), it is found that hydrogen bonding also participates in the self-assembly of the sheet.[47] A wetting experiment shows that the water contact angle of the layer formed by resorcinarene microtubes is 55.5 ± 0.9°, which further supports the fact that the MT possesses hydrophilic surfaces (Supporting Information, Figure S7). Interestingly, the MT could be used as the modified agent for gold nanoparticles; the SEM demonstrated that it was capable of capping gold nanoparticles and then forming hybrid microsheets (right). These results strongly suggested that the nanoparticles modified with the resorcinarene octahydrazide groups are able to generate sheetlike composites by the virtue of capping agents.

Subsequently, we extend the study by using the **C6−C0** (Figure 14a) as the capping agent for gold nanoparticles, and then the microsheets composed of gold nanoparticles were obtained. SEM observations (Supporting Information, Figure S8) together with XRD profile (Supporting Information, Figure S9) match well with our previous reports, which demonstrated that microsheets could be obtained. TEM experiments were carried out observing as-prepared gold nanoparticles (Figure 14b). It is clearly seen that the particle is irregular in shape, and polydisperse in size. Microsheets formed after approximately 2 h of incubation, as shown in Figure 14c and gold nanoparticles microsheets 1 μm long and 0.5 μm wide were observed. The XRD measurements of the composites showed the characteristic diffraction peaks of gold, which also proved the existence of the gold in the hybrid material (Figure 14d).

A possible structural organization is suggested by molecular modeling of the microtubes. It is proposed that two molecules initially pack tail-to-tail to form a thin sheet. Subsequently, stacking of the initial sheets leads to the formation of thicker sheets. The thick sheets make the self-assemblies lose flexible properties and therefore not prone to bend to

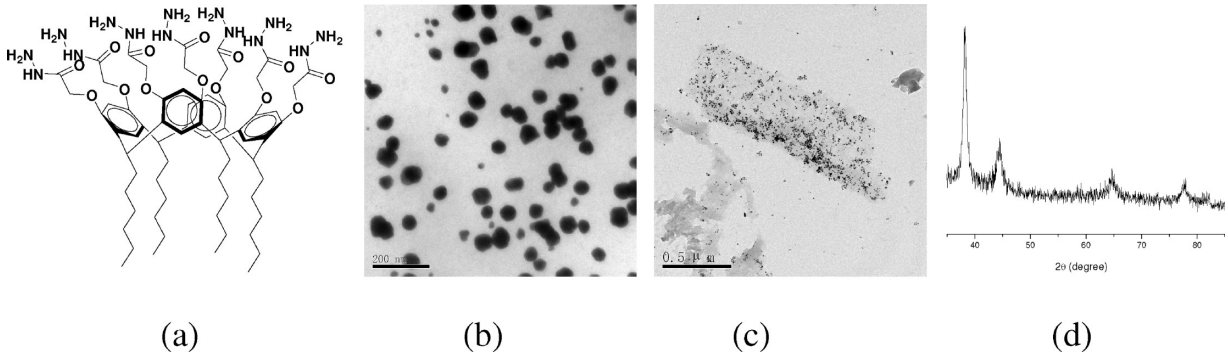

Figure 14. Diagrammatic sketch of resorcinarene C6−C0, (b) TEM image of gold nanoparticles capped by C6−C0, (c) TEM image of microsheets assembled by C6−C0, (d) XRD profile of composites.

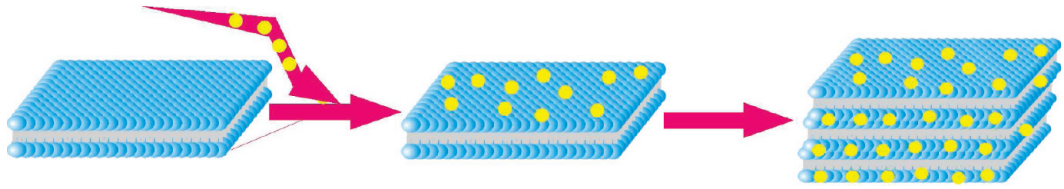

Scheme 3. Proposed schematic structure of the formation of AuNPs/microsheet. (blue, hydrophilic moieties; grey, hydrophobic moieties; yellow, AuNPs).

form a microtubule structure. Scheme 3 displays the process of NP encapsulation into microsheets. During the resorcinarene self-assembly, AuNPs were first adsorbed onto the surface of the individual thin sheets, and then the composites were obtained by each sheet piled together.

As mentioned above, the interaction between Ag/Pt/PdNPs and amino is not as strong as that of AuNPs. In this case, after replacing the amide by hydrazide groups, the resorcinarene hydrazide derivative is not a good stabilizer for modifying Ag, Pt, and Pd. The obtained NPs preferred aggregating before self-assembly. Therefore, the hybrid sheet micro-nanostructure with Ag, Pt, and Pd could not be obtained.

Release of NPs from the Hybrid Materials. As mentioned above, resorcinarene-capped NPs adsorbed to the surface of tubes by hydrogen-bond interactions. We wondered if the NPs on the tubes could be released from the hybrid materials by special treatment. To confirm this hypothesis, we used hybrid materials to explore the possibility of release. Interestingly, the suspension of composites vanished after sonication, which indicates that the NPs absorbed on the microtubes redispersed into colloids. As shown in Figure 15 left, a yellowish suspension, a purplish suspension, and a brown suspension were observed in the Ag colloids, Au colloids, and Pt colloids, respectively (top row). However, those suspensions disappeared after sonication (bottom row). Metal nanoparticles released from the tubes after sonication were displayed in Figure S10. It is noticeable that the resultant solution/mixture cannot form the inside-decorated hybrid as we obtained through the coassembly approach. Also, AuNPs could be released from the hybrid materials obtained by **C15−C2** self-assembly in the presence of AuNPs. The increase of the NP colloid concentration after sonication was demonstrated by UV−vis spectroscopy, which shows dramatic increases in absorbance. As a model system, in the experiment with AuNPs/microtubes composites, the absorbance of gold colloid increased from 0.6 to 0.9 (Figure 15, right).

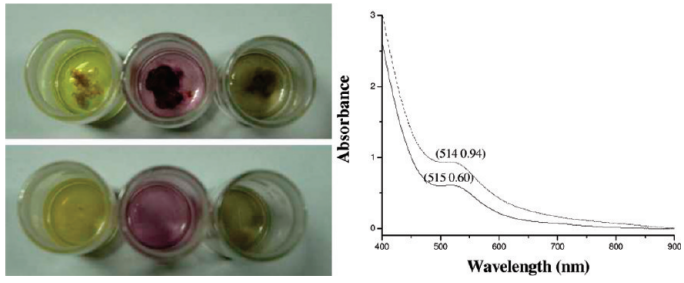

Figure 15. The optical image of sample before and after sonication (left); UV−vis spectra of gold colloid before and after sonication (right).

Figure 16 illustrates TEM images and histograms of size distribution of the released Au nanoparticles, the average size with standard deviation determined from their histograms is 4.9 ± 1.3 nm. We can see that the NPs are dispersed uniformly, each particle is separated, and no aggregation was observed. Also, the NPs absorbed in the microsheets could also be released from the assemblies by sonication. As shown in Supporting Information, Figure S11, the increase in the UV−vis spectra after treating hybrids with sonication is in accordance with the tendency of microtubules composites.

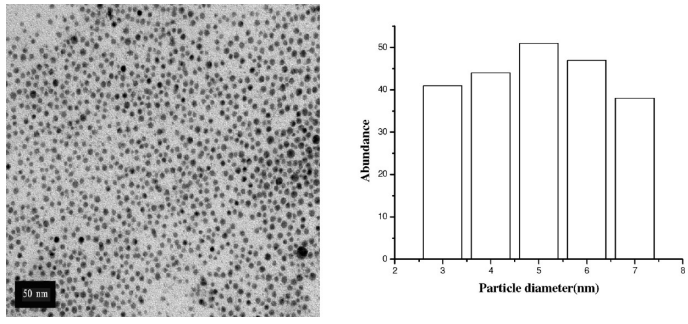

Figure 16. TEM images (left) and size histograms (right) for the gold nanoparticles redispersed from the microtube after sonication.

Proposed Illustration of Templates Method and Real-Time Encapsulation. An outline of the proposed process is shown in Scheme 4. Arrow 1 illustrates the process of adsorption by the template method. As described above, tube were initially formed by the curve of resorcinarene-based sheets. Then, microtubes incorporate abundant free amide groups on their surfaces as binding sites to anchor various nanoparticles *via* hydrogen bonds and finally accomplished the template adsorption process. Arrow 2 displays the process of NP encapsulation into microtubes during the resorcinarene self-assembly, which results in the formation of NP-loaded microtubes. During the formation of gold-wall microtubes, two steps are important. AuNPs were first adsorbed onto the surface of the multilayer sheet, and then the sheet curled into a tubular structure. This feature enables decoration of the inside and outside sur-

faces of microtubes with different NPs, which opens up various potential applications.

CONCLUSION

Resorcinarene-functionalized metal nanoparticles such as AuNPs, AgNPs, PtNPs, and PdNPs were prepared in aqueous medium. By using the microtubes as templates, hybrid materials were prepared *via* immobilizing nanoparticles onto the surface of microtubes. Interestingly, AuNPs could be incorporated into the multilayer walls of microtubes during the self-assembly process of resorcinarene. This enables the loading of various NPs on both the interior and exterior of the microtube surfaces. Furthermore, by the self-assembly of capping agent, sheetlike hybrid materials were also obtained. Interestingly, NPs adsorbed on the surface and encapsulated inside microtubes could be redispersed by sonication. This method could be customized to incorporate NPs into microtubes for separation, which will be widely applicable in selectively separation. Compared with nanoparticles dispersed in organic phases, the resorcinarene-capped nanoparticles dispersed in water are expected to have better biocompatibility and more promising applications in the future.

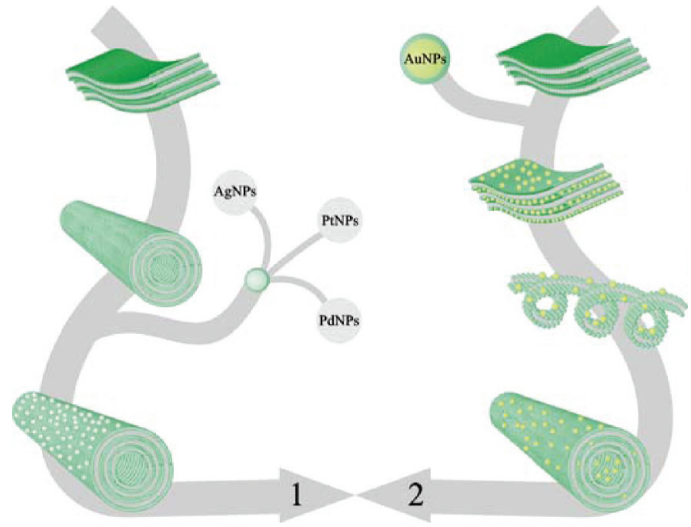

Scheme 4. Schematic representation of the formation of hybrid materials. Arrow 1: illustration of template method for preparing hybrid materials, which consists of template formation, NPs adsorption (white particles: AgNPs, PtNPs, PdNPs). Arrow 2: the AuNPs encapsulated into microtubes during the self-assembled process of C15−C2 (yellow particles, AuNPs). Green moieties, hydrophilic segment, grey moieties, hydrophobic segment

EXPERIMENTAL SECTION

Materials and Methods. Hydrochloroauric acid ($HAuCl_4$), silver nitrate ($AgNO_3$), potassium tetrachloroplatinate (II) (K_2PtCl_4), palladium(II) chloride ($PdCl_2$), and sodium borohydride ($NaBH_4$) were of reagent grade and were purchased from Shanghai Chemical Reagent Co. All polyamino amphiphilic resorcinarenes were synthesized following the procedures described in detail in previous publications.[30] Polyamino amphiphilic resorcinarenes-based microtube was prepared according to our previous reports.[47] Deionized ultrafiltered water was purified through a Milli-Q system. All glassware were cleaned with aqua regia and rinsed with deionized water.

Synthesis of AuNPs. In a typical experiment, an aqueous solution of $HAuCl_4$ (0.50 mL; 9.7 mM) and **C5−C2** (8.0 mL; 0.03 M) aqueous solution (pH = 3) were mixed in a 100 mL round flask. Then, sodium borohydride aqueous solution (1.50 mL; 0.1 M) was injected into the above solution under vigorous stirring, and the resorcinarene-capped AuNPs were immediately obtained.

Synthesis of AgNPs. The AgNPs were prepared in the following manner: 0.1 mL of 9.7 mM $AgNO_3$ and 6 mL of 200 μM resorcinarene **C5−C2** aqueous solution were mixed and allowed to stir for 2 min. To this transparent solution, 0.1 mL of 2 M HNO_3 was added followed by the addition of 0.4 mL of 0.1 M $NaBH_4$ solution. It could be seen that the colorless solution initially became yellowish then turned to bright yellow, indicating the formation of AgNPs.

Synthesis of PtNPs. A 0.8 mL portion of 4.8 mM K_2PtCl_6 and 6 mL of 200 μM resorcianrene **C5−C2** aqueous solution were mixed and allowed to stir for 2 min. To this was added 0.1 mL of 2 M HCl to adjust the pH to 2. Then, 0.6 mL of 0.1 M $NaBH_4$ solution was injected to the mixtures under stirring, which resulted in the generation of the platinum nanoparticles.

Synthesis of PdNPs. A 1.2 mL portion of 1.4 mM $PdCl_2$ and 6 mL of 200 μM resorcianrene **C5−C2** aqueous solution were mixed and allowed to stir for 2 min; 0.6 mL of 0.1 M $NaBH_4$ solution was injected in to the mixture under stirring, which resulted in the formation of the palladium particles.

Formation of C15−C2-based Self-Assemblies in Water. C15−C2 was acidified with hydrochloric acid to give 3×10^{-4} M aqueous solution (pH = 4). Subsequently, the obtained solution was diluted with distilled water to produce **C15−C2** solutions of concentrations at 1.5×10^{-4} M, which were aged at room temperature at least for 4 weeks.

Formation of (C6−C0/−C0)-Based Microsheets in Water. C6−C0 was acidified with hydrochloric acid to give 3×10^{-4} M aqueous solution (pH <1). Subsequently, the obtained solution was diluted with distilled water to produce **C6−C0** solutions of concentrations at 1.5×10^{-4} M, which were aged at room temperature at least for 2 h.

Template Method: Decoration of Ag, Pt, and Pd NPs onto Resorcinarene-Based Microtubes. The suspension of resorcinarene microtubes were immersed in silver colloids, platinum colloids, and palladium colloids, respectively. It was clearly shown that the initial white suspension was converted into a colorful suspension after aging for several days, which suggested the formation of the nanoparticle-coated microtubes. The obtained composites were then rinsed twice with deionized water.

Co-assembly Method: Fabrication of Aunps Loaded Resorcinarene Microtubes. An aqueous solution of 0.4 mL of 9.7 mM $HAuCl_4$ and 6 mL of 150 μM resorcinarene **C15−C2** solution (pH = 4) were mixed. Then, 0.4 mL of 0.1 M $NaBH_4$ aqueous solution was injected into the mixtures under stirring, and the colloidal gold was immediately obtained. In a typical experiment, the pH of as-preparaed gold colloids was adjusted to 4 with 2 M hydrochloric acid. Consequently, the AuNPs were loaded into the microtube by the self-assembly of the resorcinarene in gold colloids.

Separation of the Different Nanoparticles. For the separation of metal nanoparticles from microtubular supports, the suspension was drawn from the mixture and the hybrid was washed with distilled water three times followed by the addition of water. Subsequently, the obtained sample was treated by sonication for 5 min for further charaterization.

Methods. UV−vis spectroscopy was measured on a Shimadzu UV-2501 PC UV−visible spectrometer. The spectral background absorption was subtracted by means of the UV−vis spectrum of water. The TEM images were obtained using a Philips TECNAI-12 instrument with an accelerating voltage of 120 kV. The ultrathin section of microtube was placed on copper grids coated with formavar. Before ultramicrotomy, fresh microtube specimens were

prefixed with 2.5% glutaraldehyde and the specimens were subsequently postfixed with 1% osmium tetroxide. Dehydrated by a graded series of ethanol and acetone, the specimens infiltrated an Epon 812 mixture and were embedded. FE-SEM was applied to investigate the morphology, which was carried out with a Hitachi S-4800 field emission scanning electron microscopy. EDX was examined by SEM (XL-30) instrument. XRD data were obtained with a graphite monochromatic device and Cu Kα radiation (λ = 0.15406 nm) on the D8 Advance superspeed powder diffractometer (Bruker), operated in the θ:2θ mode primarily in the 20−85° (2θ) range and step-scan of 2θ = 0.04°. The tube voltage was 80 kV, and the tube current was 200 mA.

Acknowledgment. This work was financially supported by the National Natural Science Foundation of China (Grant Nos. 20672091 and 20773105). The authors also acknowledge W.-D. Zhou and Y.-F. Chen for SEM and TEM experiments.

Supporting Information Available: FT-IR and UV−vis spectra, XRD profile, SEM and TEM images of resorcinarene-based aggregates, contact angle experiment. This material is available free of charge *via* the Internet at http://pubs.acs.org.

REFERENCES AND NOTES

1. Sharma, J.; Chhabra, R.; Cheng, A.; Brownell, J.; Liu, Y.; Yan, H. Control of Self-Assembly of DNA Tubules through Integration of Gold Nanoparticles. *Science* **2009**, *323*, 112–116.
2. Lim, B.; Jiang, M.; Camargo, P. H. C.; Cho, E. C.; Tao, J.; Lu, X.; Zhu, Y.; Xia, Y. Pd−Pt Bimetallic Nanodendrites with High Activity for Oxygen Reduction. *Science* **2009**, *324*, 1302–1305.
3. Tao, F.; Grass, M. E.; Zhang, Y.; Buther, D. R.; Renzas, J. R.; Lin, Z.; Chung, J. Y.; Mun, B. S.; Salmeron, M.; Somorjai, G. A. Reaction-Driven Restructuring of Rh-Pd and Pt−Pd Core−Shell Nanoparticles. *Science* **2008**, *322*, 932–934.
4. Herzing, A. A.; Kiely, C. J.; Carley, A. F.; Landon, P.; Hutchings, G. J. Identification of Active Gold Nanoclusters on Iron Oxide Supports for CO Oxidation. *Science* **2008**, *321*, 1331–1335.
5. Li, W.; Camargo, P. H. C.; Lu, X.; Xia, Y. Dimers of Silver Nanospheres: Facile Synthesis and Their Use as Hot Spots for Surface-Enhanced Raman Scattering. *Nano Lett.* **2009**, *9*, 485–490.
6. Cobley, C. M.; Rycenga, M.; Zhou, F.; Li, Z.-Y.; Xia, Y. Controlled Etching as a Route to High Quality Silver Nanospheres for Optical Studies. *J. Phys. Chem. B* **2009**, *113*, 16975–16982.
7. Sun, Y.; Xia, Y. Shape-Controlled Synthesis of Gold and Silver Nanoparticles. *Science* **2002**, *298*, 2176–2179.
8. Yavuz, M. S.; Cheng, Y.; Chen, J.; Cobley, C. M.; Zhang, Q.; Rycenga, M.; Xie, J.; Kim, C.; Song, K.; Schwartz, A. G.; *et al.* Gold nanocages covered by smart polymers for controlled release with near-infrared light. *Nat. Mater.* **2009**, *8*, 925–939.
9. Quiros, I.; Yamada, M.; Kubo, K.; Mizutani, J.; Kurihara, M.; Nishihara, H. Preparation of Alkanethiolate-Protected Palladium Nanoparticles and Their Size Dependence on Synthetic Conditions. *Langmuir* **2002**, *18*, 1413–1418.
10. Chen, S.; Huang, K.; Stearns, J. A. Alkanethiolate-Protected Palladium Nanoparticles. *Chem. Mater.* **2000**, *12*, 540–541.
11. Templetion, A. C.; Hostetler, M. J.; Kraft, C. T.; Murray, R. W. Reactivity of Monolayer-Protected Gold Cluster Molecules: Steric Effects. *J. Am. Chem. Soc.* **1998**, *120*, 1906–1911.
12. Chen, X. Y.; Li, J. R.; Jiang, L. Two-Dimensional Arrangement of Octadecylamine-Functionalized Gold Nanoparticles Using the LB Technique. *Nanotechnology* **2000**, *11*, 108–111.
13. Hussain, I.; Brust, M.; Papworth, A. J.; Cooper, A. I. Preparation of Acrylate-Stabilized Gold and Silver Hydrosols and Gold-Polymer Composite Films. *Langmuir* **2003**, *19*, 4831–4835.
14. Zhang, J.; Liu, H.; Wang, Z.; Ming, N. Shape-Selective Synthesis of Gold Nanoparticles with Controlled Sizes, Shapes, and Plasmon Resonances. *Adv. Funct. Mater.* **2007**, *17*, 3295–3303.
15. Balasubramanian, R.; Kwon, Y.-G.; Wei, A. Encapsulation and Functionalization of Nanoparticles in Crosslinked Resorcinarene Shells. *J. Mater. Chem.* **2007**, *17*, 105–112.
16. Guerrini, L.; Garcia-Ramos, J. V.; Domingo, C.; Sanchez-Cortes, S. Functionalization of Ag Nanoparticles with Dithiocarbamate Calix[4]arene as an Effective Supramolecular Host for the Surface-Enhanced Raman Scattering Detection of Polycyclic Aromatic Hydrocarbons. *Langmuir* **2006**, *22*, 10924–10926.
17. Jin, T.; Fujii, F.; Yamada, E.; Nodasaka, Y.; Kinjo, M. Control of the Optical Properties of Quantum Dots by Surface Coating with Calix[*n*]arene Carboxylic Acids. *J. Am. Chem. Soc.* **2006**, *128*, 9288–9289.
18. Misra, T. K.; Chen, T.-S.; Liu, C.-Y. Phase Transfer of Gold Nanoparticles from Aqueous to Organic Solution Containing Resorcinarene. *J. Colloid Interface Sci.* **2006**, *297*, 584–588.
19. Tripp, S. L.; Pusztay, S. V.; Ribbe, A. E.; Wei, A. Self-Assembly of Cobalt Nanoparticle Rings. *J. Am. Chem. Soc.* **2002**, *124*, 7914–7915.
20. Kim, B.; Tripp, S. L.; Wei, A. Self-Organization of Large Gold Nanoparticle Arrays. *J. Am. Chem. Soc.* **2001**, *123*, 7955–7956.
21. Jin, T.; Fujii, F.; Sakata, H.; Tamura, M.; Kinjo, M. Amphiphilic *p*-Sulfonatocalix[4]arene-Coated CdSe/ZnS Quantum Dots for the Optical Detection of the Neurotransmitter Acetylcholine. *Chem. Commun.* **2005**, 4300–4302.
22. Stavens, K. B.; Pusztay, S. V.; Zou, S.; Andres, R. P.; Wei, A. Encapsulation of Neutral Gold Nanoclusters by Resorcinarenes. *Langmuir* **1999**, *15*, 8337–8339.
23. Wei, A. Calixarene-Encapsulated Nanoparticles: Self-Assembly into Functional Nanomaterials. *Chem. Commun.* **2006**, 1581–1591.
24. Huc, V.; Pelzer, K. A New Specifically Designed Calix[8]arene for the Synthesis of Functionalized, Nanometric and Subnanometric Pd, Pt, and Ru Nanoparticles. *J. Colloid Interface Sci.* **2008**, *318*, 1–4.
25. Gedanken, A.; Ben-Ishay, M. L. A New Specifically Designed Calix[8]arene for the Synthesis of Functionalized, Nanometric and Subnanometric Pd, Pt and Ru Nanoparticles. *Langmuir* **2007**, *23*, 5238–5242.
26. Misra, T. K.; Liu, C.-Y. Synthesis, Isolation, And Redispersion of Resorcinarene-Capped Anatase TiO_2 Nanoparticles in Nonaqueous Solvents. *J. Colloid Interface Sci.* **2007**, *310*, 178–183.
27. Chin, S. F.; Makha, M.; Raston, C. L.; Saunders, M. Magnetite Ferrofluids Stabilized by Sulfonato-calixarenes. *Chem. Commun.* **2007**, 1948–1950.
28. Ha, J.-M.; Solovyov, A.; Katz, A. Postsynthetic Modification of Gold Nanoparticles with Calix[4]arene Enantiomers: Origin of Chiral Surface Plasmon Resonance. *Langmuir* **2009**, *25*, 153–158.
29. Guerrini, L.; Garcia-Ramos, J. V.; Domingo, C.; Sanchez-Cortes, S. Self-Assembly of a Dithiocarbamate Calix[4]arene on Ag Nanoparticles and Its Application in the Fabrication of Surface-Enhanced Raman Scattering Based Nanosensors. *Phys. Chem. Chem. Phys.* **2009**, *11*, 1787–1793.
30. Shen, M.; Sun, Y.; Han, Y.; Yao, R.; Yan, C. G. Strong Deaggregating Effect of a Novel Polyamino Resorcinarene Surfactant on Gold Nanoaggregates under Microwave Irradiation. *Langmuir* **2008**, *24*, 13161–13167.
31. Chen, M.; Diao, G. W.; Li, C. H.; Zhou, X. M. Phase Transition of Silver Nanoparticles from Aqueous Solution to Chloroform with the Help of Inclusion Complexes of *p*-Sulfonated Calix[4]arene and Alkanethiol Molecules and Its Application in the Size Sorting of Nanoparticles. *Nanotechnology* **2007**, *18*, 175706.
32. Li, H.; Qu, F. Synthesis of CdTe Quantum Dots in Sol-Gel-Derived Composite Silica Spheres Coated with Calix[4]arene as Luminescent Probes for Pesticides. *Chem. Mater.* **2007**, *19*, 4148–4154.

33. Li, H.; Qu, F. Selective Inclusion of Polycyclic Aromatic Hydrocarbons (PAHs) on Calixarene-Coated Silica Nanospheres Englobed with CdTe Nanocrystals. *J. Mater. Chem.* **2007**, *17*, 3536–3544.
34. Wei, A.; Kim, B.; Sadtler, B.; Tripp, S. L. Tunable Surface-Enhanced Raman Scattering from Large Gold Nanoparticle Arrays. *Chemphyschem* **2001**, *12*, 743–745.
35. Tripp, S. L.; Dunin-Borkowski, R. E.; Wei, A. Flux Closure in Self-Assembled Cobalt Nanoparticle Rings. *Angew. Chem.* **2003**, *115*, 5749–5751.
36. Shen, M.; Chen, W. F.; Sun, Y.; Yan, C. G. Synthesis and Characterization of Water-Soluble Gold Colloids Stabilized with Aminoresorcinarene. *J. Phy. Chem. Sol.* **2007**, *68*, 2252–2261.
37. Tshikhudo, T. R.; Demuru, D.; Wang, Z.; Brust, M.; Secchi, A.; Arduini, A.; Pochini, A. Molecular Recognition by Calix[4]arene-Modified Gold Nanoparticles in Aqueous Solution. *Angew. Chem., Int. Ed.* **2005**, *44*, 2913–2916.
38. Jin, T.; Fujii, F.; Sakata, H.; Tamura, M.; Kinjo, M. Calixarene-Coated Water-Soluble CdSe−ZnS Semiconductor Quantum Dots That Are Highly Fluorescent and Stable in Aqueous Solution. *Chem. Commun.* **2005**, 2829–2831.
39. Hammond, P. T. Bridging Macro and Nano. *ACS Nano* **2009**, *3*, 485–486.
40. Tristany, M.; Moreno-Manas, M.; Pleixats, R.; Chaudret, B.; Philippot, K.; Dieudonne, P.; Lecante, P. Formation of Nanocomposites of Platinum Nanoparticles Embedded into Heavily Fluorinated Aniline and Displaying Long Range Organization. *J. Mater. Chem.* **2008**, *18*, 660–666.
41. Vemula, P. K.; Aslam, U.; Mallia, V. A.; John, G. In Situ Synthesis of Gold Nanoparticles Using Molecular Gels and Liquid Crystals from Vitamin-C Amphiphiles. *Chem. Mater.* **2007**, *19*, 138–140.
42. Bhat, S.; Maitra, U. Nanoparticle-Gel Hybrid Material Designed with Bile Acid Analogues. *Chem. Mater.* **2006**, *18*, 4224–4226.
43. Ray, S.; Das, A.; Banerjee, K. A. Smart oligopeptide gels: in situ formation and stabilization of gold and silver nanoparticles within supramolecular organogel networks. *Chem. Commun.* **2006**, 2816–2818.
44. Song, Y.; Challa, S. R.; Medforth, C. J.; Qiu, Y.; Watt, R. K.; Pena, D.; Miller, J. E.; Swol, F. v.; Shelnutt, J. A. Synthesis of peptide-nanotube platinum-nanoparticle composites. *Chem. Commun.* **2004**, 1044–1045.
45. Kong, H.; Jang, J. Antibacterial Properties of Novel Poly(methyl methacrylate) Nanofiber Containing Silver Nanoparticles. *Langmuir* **2008**, *24*, 2051–2056.
46. Krack, M.; Hohenberg, H.; Kornowski, A.; Lindner, P.; Weller, H.; Forster, S. Nanoparticle-Loaded Magnetophoretic Vesicles. *J. Am. Chem. Soc.* **2008**, *130*, 7315–7320.
47. Sun, Y.; Yan, C. G.; Yao, Y.; Han, Y.; Shen, M. Self-Assembly and Metallization of Resorcinarene Microtubes in Water. *Adv. Funct. Mater.* **2008**, *18*, 3981–3990.
48. Aslan, K.; Perez-Luna, V. H. Surface Modification of Colloidal Gold by Chemisorption of Alkanethiols in the Presence of a Nonionic Surfactant. *Langmuir* **2002**, *18*, 6059–6065.
49. Kemp, M. M.; Kumar, A.; Mousa, S.; Park, T.-J.; Ajayan, P.; Kubotera, N.; Mousa, S. A.; Linhardt, R. J. Synthesis of Gold and Silver Nanoparticles Stabilized with Glycosaminoglycans Having Distinctive Biological Activities. *Biomacromolecules* **2009**, *10*, 589–595.
50. Tian, Z. Q.; Jiang, S. P.; Liu, Z.; Li, L. Polyelectrolyte-Stabilized Pt Nanoparticles As New Electrocatalysts for Low Temperature Fuel Cells. *Electrochem. Commun.* **2007**, *9*, 1613–1618.
51. Teranishi, T.; Miyake, M. Size Control of Palladium Nanoparticles and Their Crystal Structures. *Chem. Mater.* **1998**, *10*, 594–600.
52. Lin, Y.; Watson, K. A.; Fallbach, M. J.; Ghose, S.; Smith, J. G.; Delozier; Jr, D. M.; Cao, W.; Crooks, R. E.; Connell, J. W. Rapid, Solventless, Bulk Preparation of Metal Nanoparticle-Decorated Carbon Nanotubes. *ACS Nano* **2009**, *3*, 871–884.
53. Huang, S. Y.; Chang, S. M.; Yeh, C. T. Characterization of Surface Composition of Platinum and Ruthenium Nanoalloys Dispersed on Active Carbon. *J. Phys. Chem. B* **2006**, *110*, 234–239.
54. Kim, S.-W.; Park, J.; Jang, Y.; Chung, Y.; Hwang, S.; Hyeon, T. Synthesis of Monodisperse Palladium Nanoparticles. *Nano Lett.* **2003**, *3*, 1289–1291.
55. Kunio, E.; Ryoko, I. Tomokazu. Preparation of PAMAM- and PPI-Metal (Silver, Platinum, and Palladium) Nanocomposites and Their Catalytic Activities for Reduction of 4-Nitrophenol. *Langmuir* **2004**, *20*, 237–243.
56. Kunio, E.; Akihiro, S.; Atsushi, Y.; Kanjiro, T. Role of Poly(amidoamine) Dendrimers for Preparing Nanoparticles of Gold, Platinum, and Silver. *Langmuir* **2000**, *16*, 2604–2608.
57. Kuo, P.; Chen, W. Formation of Silver Nanoparticles under Structured Amino Groups in Pseudo-dendritic Ploy(allylamine) Derivatives. *J. Phys. Chem. B* **2003**, *107*, 11267–11272.
58. Gao, P.; Liu, M. Compression Induced Helical Nanotubes in a Spreading Film of a Bolaamphiphile at the Air/Water Interface. *Langmuir* **2006**, *22*, 6727–6729.
59. Zhou, Y.; Shimizu, T. Lipid Nanotubes: A Unique Template To Create Diverse One-Dimensional Nanostructures. *Chem. Mater.* **2008**, *20*, 625–633.
60. Zhan, C.; Gao, P.; Liu, M. Self-Assembled Helical Spherical-Nanotubes from an L-Glutamic Acid Based Bolaamphiphilic Low Molecular Mass Organogelator. *Chem. Commun.* **2005**, 462–464.
61. Shimizu, T.; Masuda, M.; Minamikawa, H. Supramolecular Nanotube Architectures Based on Amphiphilic Molecules. *Chem. Rev.* **2005**, *105*, 1401.
62. Lu, Y.; Mei, Y.; Drechsler, M.; Ballauff, M. Thermosensitive Core−Shell Particles as Carriers for Ag Nanoparticles: Modulating the Catalytic Activity by a Phase Transition in Networks. *Angew. Chem., Int. Ed.* **2006**, *45*, 813–816.
63. Klaus, T.; Joerger, R.; Olsson, E.; Granqvist, C.-G. Silver-Based Crystalline Nanoparticles, Microbially Fabricated. *Proc. Natl. Acad. Sci. U.S.A.* **1999**, *96*, 13611–13614.
64. Wang, L.; Guo, S.; Huang, L.; Dong, S. Alternate Assemblies of Polyelectrolyte Functionalized Carbon Nanotubes and Platinum Nanoparticles as Tunable Electrocatalysts for Dioxygen Reduction. *Electrochem. Commun.* **2007**, *9*, 827–832.
65. Klajn, R.; Gray, T. P.; Wesson, P. J.; Myers, B. D.; Dravid, V. P.; Smoukov, S. K.; Grzybowski, B. A. Bulk Synthesis and Surface Patterning of Nanoporous Metals and Alloys from Supraspherical Nanoparticle Aggregates. *Adv. Funct. Mater.* **2008**, *18*, 2763–2769.
66. Wu, S.; Wu, J.; Liu, Y.; Ju, H. Conductive and Highly Catalytic Nanocage for Assembly and Improving Function of Enzyme. *Chem. Mater.* **2008**, *20*, 1397–1403.